NewSOL Project (720985)

Implementation and validation tests for Fluent: Case 0

Victor Seram

Margarida Giestas Lima

Pedro Azevedo

December, 2018

Estrada do Paço do Lumiar, 22
1649-038 LISBOA - Portugal
Tel: +351 210 924 600/1
Fax: +351 217 166 966 online:217166966@fax.ptprime.pt
www.lneg.pt

Copyright notice

LEN-UER-2018-N11-IR
"Implementation and validation tests for Fluent: Case 0"
Internal Report on work developed by LNEG included in Subtask 5.1 "Thermocline concrete tank simulation" for partial fulfillment of deliverable D5.1 "System configuration for thermocline concrete tank".
Victor Seram, Margarida Giestas and Pedro Azevedo
December, 2018

Table of contents

List of figures

List of tables

1. Introduction

The present report was made according to the implementation of "Fluent: Case 0"[1] of the NewSol Project (Grant nº 720985). The Ansys computational package software was used for the conducted simulations. A 2D geometry symmetrical at the middle axis was constructed. Several meshes were both made and simulated for the minimum computational cost. For simplicity of the problem and at this early stage of development of the model, the ullage space was taken to be filled with HTF (Heat Transfer Fluid). Although HTF fills the ullage space in the tank, this is not in good agreement with the condition described in Case 0 which considers air as the medium. All the simulations were performed with steady state conditions. However, in the future transient state would be used.

Two turbulent models: k-ε (Enhanced Wall Function) and k-ω (Shear-Stress Transport) were tested regarding the accuracy of the results near the wall and also with respect to the minimum computational cost. Grid size independence, initial solution independence and convergence tests were also performed with the selected mesh.

2. Geometry

A 2D structure of the tank was designed with DesignModeler from the computational software package Ansys. The structure was developed in the x-y axis. The tank was divided into 9 equal parts, 8 MS/filler material zones (parts 2 to 9) and 1 zone as the ullage space (Part 1). The individual parts were named as part 1 to part 9 according to the sequence from the top as shown in Figure 2.1 below.

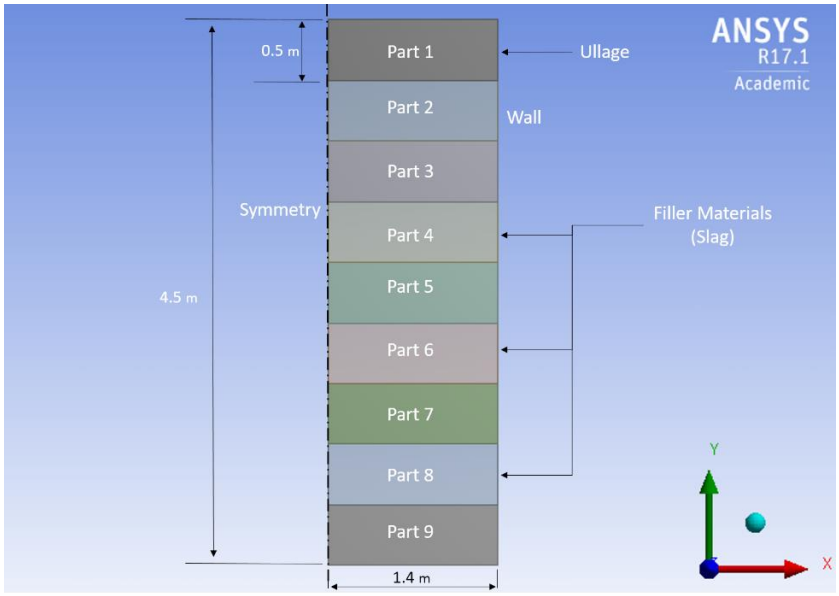

Figure 2.1: Detailed structure of the geometry.

[1] P. Azevedo, 2018, "*Fluent: Case 0*", Internal Report on work developed by LNEG included in Subtask 5.1 "*Thermocline concrete tank simulation*" for partial fulfillment of deliverable D5.1 "*System configuration for thermocline concrete tank*", LEN-UER-2018-N08-IR, May, 2018

The geometry was considered a symmetrical design with a mirror plane in the longitudinal axis, thus the x-axis represents the radius of the tank. The tank has 4,5 m in height and a radius of 1,4 m. Each zone has 0,5 m in height. Parts 4, 6 and 8 were considered as the baskets with possibility of having filler material (slag from S. Domingos Mines). For this particular case, the ullage space was also filled with the HTF (Heat Transfer Fluid).

For the charging process the HTF is introduced at the top of the tank and exits from the bottom end. The process is reversed for the discharging process, the HTF is introduced at the bottom of the tank and exits at the top.

3. Mesh

Due to simplicity of the geometry and, mainly to the unidirectional tendency of the flow, a structured grid was considered instead of an unstructured grid. A sizing function was applied at the wall, symmetry and the interfaces between the parts of the structure dividing the geometry into various equal parts to form a properly structured mesh. A radial resolution of 5 mm (280 cells) and a vertical resolution of 5 mm (900 cells) were considered. The mesh resulting from these resolutions rises to 252,0 k cells.

In order to increase accuracy of calculations near wall region (a Y^+ value below 1 was aimed) and better convergence during the turbulent flow a Wall of Inflation (WoI) was considered. Thus, a 15 layered wall of inflation was constructed. This resulted in an expectedly improved mesh with 263,7 k cells. A magnified view of the inflation at the wall is shown along with the structured mesh of the geometry in the Figure 3.1.

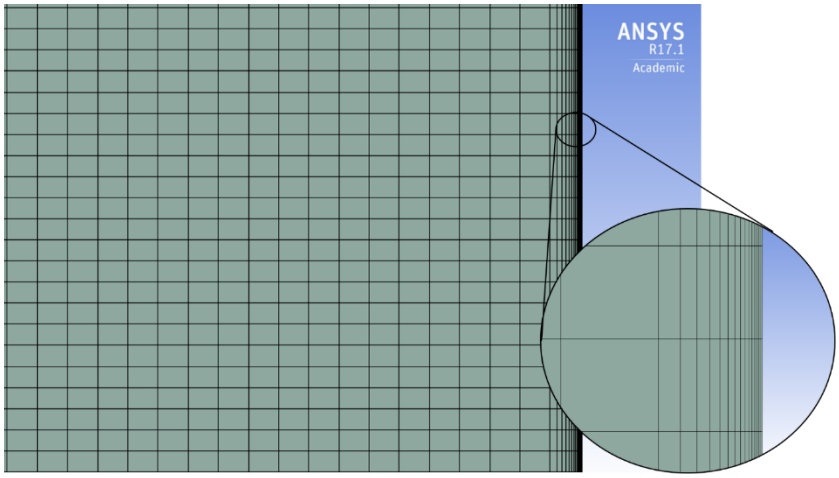

Figure 3.1: Structured mesh with magnified view of the inflation at the wall.

4. Models

Considering the flow's turbulence as isotropic, models such as RSM or LES where discarded. A single equation turbulence model such as Spalart-Allmaras and the inviscid formulation were also discarded.

Two models were tested for the flow calculation along the tank.

- k-ε (with wall enhanced function); and
- k-ω (Shear-Stress Transfer).

A similar structured mesh with 263,7 k cells was used for both the models. This mesh was tested with similar initial conditions while charging the tank. The convergence criteria considered assumed the form of a maximum amount of added residuals. The residual values considered in the convergence criteria are shown in Table 4.1.

Table 4.1: Values of the residuals for the convergence criteria.

Continuity	x	y	Energy	k	ε/ω
10e-3	10e-3	10e-3	10e-6	10e-3	10e-3

While testing both turbulence models, the Y^+ value near the wall with the k-ε (with wall enhanced function) showed some fluctuations above 1,0, while the Y^+ value at the wall with k-ω (SST) showed a stable value. Those results are presented in Figure 4.1.

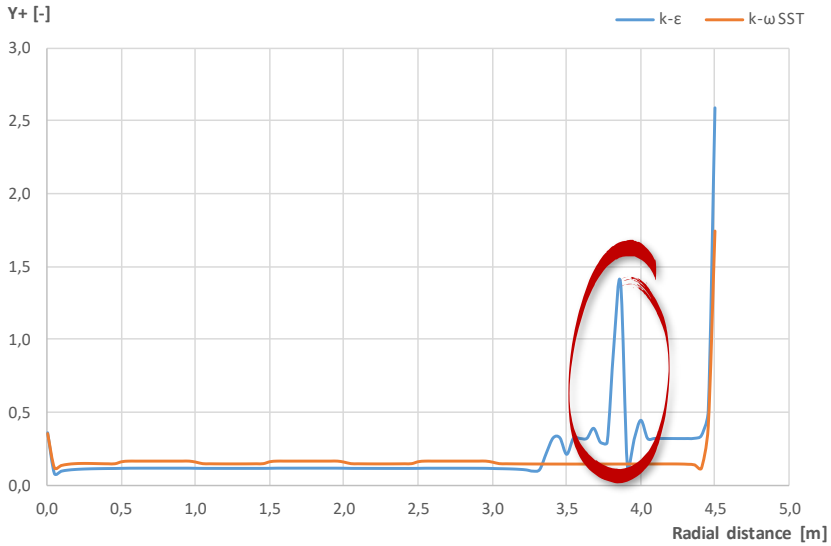

Figure 4.1: Turbulence production for both k-ε (with wall enhanced function) and k-ω (SST).

With regard to the computational effort, the number of iterations in order to achieve convergence is higher for the k-ε (with wall enhanced function) model without the Wall of Inflation than with it (the effect of the increased mesh is already included) and the number of iterations to achieve convergence with the k-ω (SST) is even lower. Table 4.2 presents the relative results of these calculations.

Table 4.2: Computational effort of the considered turbulence models.

Parameter	k-ε	k-ε (WoI)	k-ω (SST)
# of cells	252,0 k	263,7 k	263,7 k
Relative time	100%	72,1%	57,4%

Hence, due to better Y^+ values leading to reliable turbulent flow calculations near the wall and lower computational costs the chosen model was k-ω (SST).

5. Tests

5.1. Grid size independence:

Various meshes, namely 17 meshes, were created and simulated with different sizes were starting with a vertical and radial resolution of 5 mm, respectively 900 axial cells and 280 radial cells, giving rise to a 263,7 k mesh to a vertical and radial resolution of, respectively, 1,37 mm and 2,48 mm, giving rise to a 1.902,0 k mesh. Table 5.1 shows the all the meshes and the divisions made with respect to the model.

Table 5.1: Simulated mesh number with axial and radial division.

Mesh. No.	# cells	Radial division	Axial division
1.	263700	280	900
2.	339120	300	1080
3.	402480	330	1170
4.	538560	360	1440
5.	638280	380	1620
6.	745200	400	1800
7.	801360	410	1890
8.	859320	420	1980

9.	919080	430	2070
10.	1012095	445	2115
11.	1109160	460	2340
12.	1210275	475	2475
13.	1315440	490	2610
14.	1424655	505	2745
15.	1655235	535	3015
16.	1776600	550	3150
17.	1902015	565	3285

In order to compare the behavior of these meshes against each other, 100 points on the symmetrical boundary was taken for each mesh to compare with respect to the velocity magnitude. Figure 5.1 shows the results of 7 meshes ranging from 263,7 k cells to 1109,2 k cells.

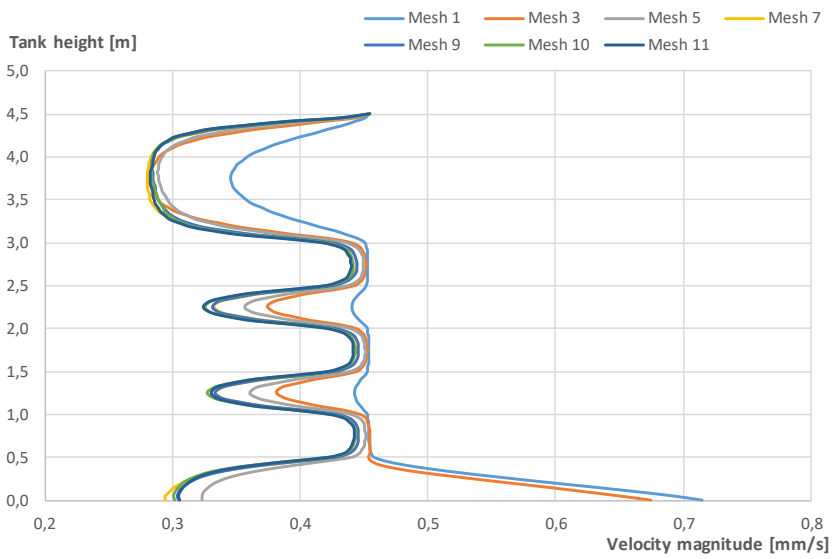

Figure 5.1: Velocity along the symmetry with respect to different mesh sizes.

According to the Figure 5.1, the curve trend changes after Mesh 3 in the outlet region (bottom part of the image). The trend in the curves tend to overlap after Mesh 7. However, to quantify the differences between all the meshes, a numerical comparison was performed with respect to all the meshes.

A velocity magnitude difference was calculated between two adjacent cells in the symmetry boundary. The summation of the difference per mesh number was then calculated and then compared with each other. The bar graph shown in Figure 5.2 is the depiction of the summation of the difference per unit mesh.

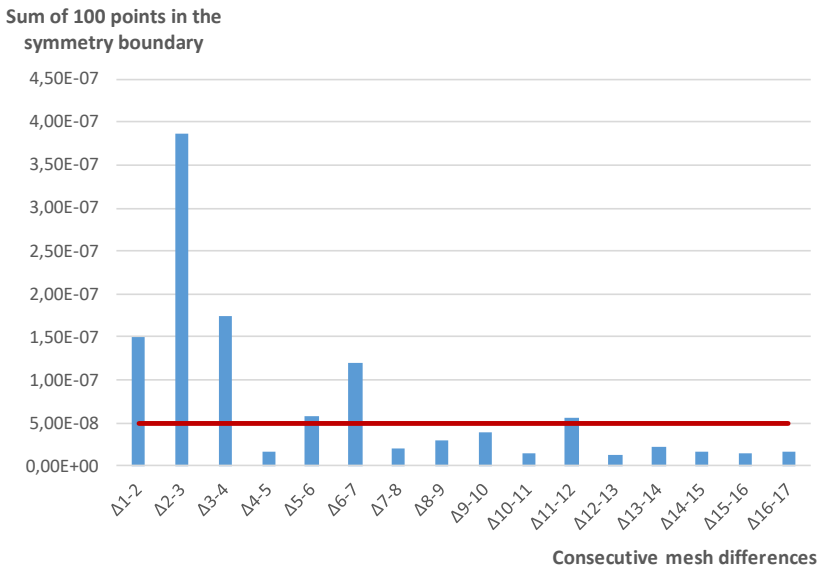

Figure 5.2: Summation of difference per unit mesh with regard to the adjacent mesh.

In order to select the preferable mesh, a numerical threshold of 5e-8 for the difference in the summation of the velocity magnitude was considered as an appropriate quantity to define the most suitable mesh. This threshold is also presented in Figure 5.2

After the 6th bar, the graph shows no crossing from the threshold 5e-8 limit (except at 11th bar, that marginally reached the threshold value). The 6th bar is the difference between the adjacent meshes 6 and 7. Thus, the selected mesh was Mesh #7 with 801,4 k cells.

5.2 Initial solution independence and convergence test:

The previous simulations were conducted with the following initial conditions:

- x-velocity: 0;
- y-velocity: 0; and
- fluid/filler temperature: 200 ˚C.

To conduct the initial solution independent tests, the temperature and y-velocity boundary conditions at the fluid inlet were set to, respectively, **500 ˚C** and **-0,4542 mm/s** and the convergence criteria were considered as described in Table 4.1.

Hence, in order to test the mesh independence with regard the initial solutions, several initial conditions were defined, with respect to y-velocity and temperature, as shown in both Table 5.2 and Table 5.3.

Table 5.2. Initial condition: Temperature.

	y-velocity (m/s)	Temperature (°C)
IS 1	0,0	500
IS 2		350
IS 3		-100
IS 4		750

Table 5.3. Initial condition: y-velocity.

	y-velocity (m/s)	Temperature (°C)
IS 5	-0,005	200
IS 6	-0,05	
IS 7	-0,5	
IS 8	-5	
IS 9	5	

The convergence was achieved for all initial solutions and the results are presented in the form of temperature profiles along both the symmetry axle and along a virtual vertical line defined at 0,7 m from the center of the tank (distance from the longitudinal axis).

In Figure 5.3 and 5.4, temperature profiles along the tank height are plotted, respectively, along the symmetry axis and at 0,7 m from the symmetry axis of the tank for all temperature and y-velocity initial conditions.

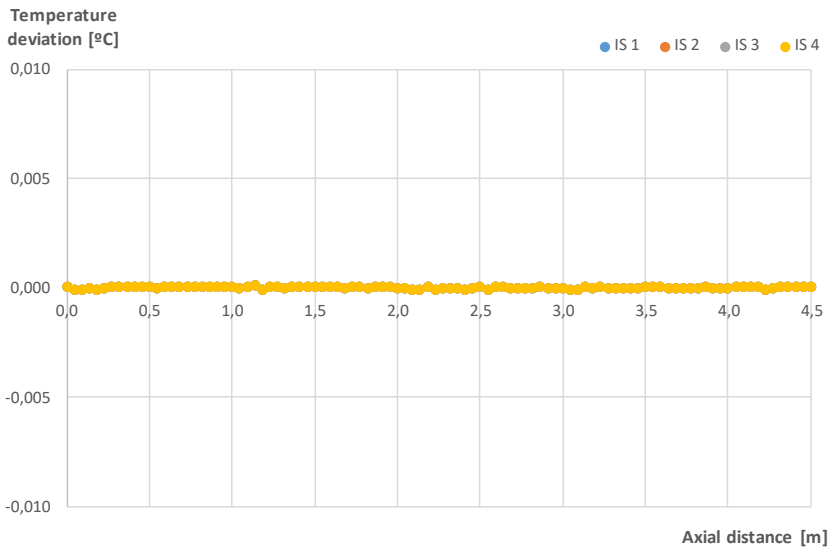

Figure. 5.3: Temperature profile along the symmetry of the tank with different initial solutions (IS) with regard to temperature.

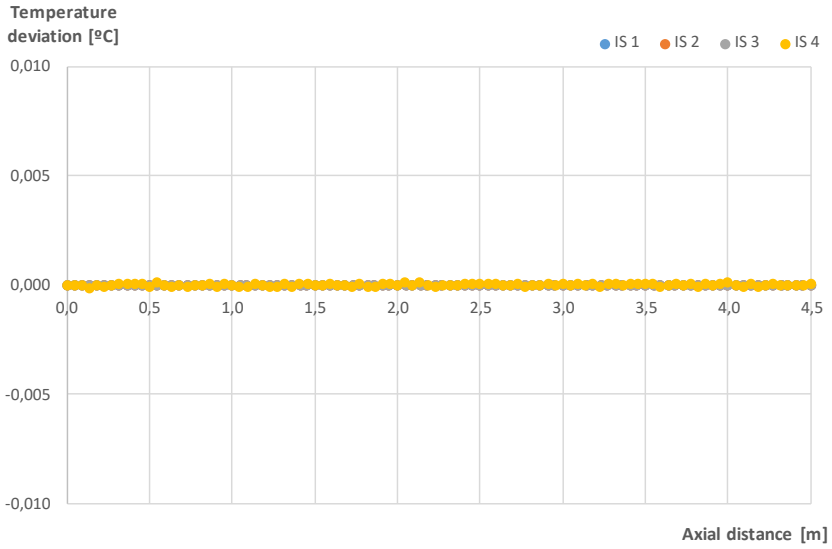

Figure. 5.4: Temperature profile along a distance of 0,7 m from the symmetry axis with different initial solutions (IS) with regard to temperature.

Considering both the Figures 5.3 and 5.4, the temperature plots completely coincide with each other, hence it can be concluded that initial convergence test for different initial temperature is successfully concluded.

However, for the initial solutions from Table 5.3 (y-velocity), a temperature gradient inside the tank ranging from 200 °C to 500 °C was found (Figure 5.5). The reason behind this behavior was considered to be the shallow convergence criteria, yielding not enough iterations in order to the inlet conditions influence the initial conditions inside the tank.

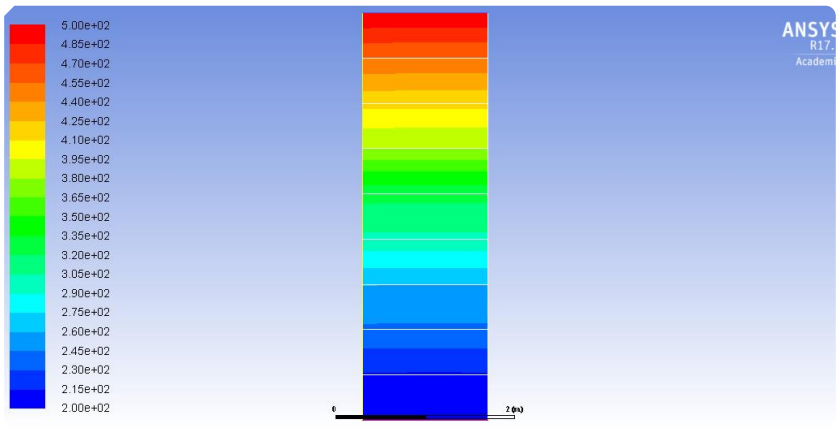

Figure 5.5: Temperature contour for initial HTF velocity -0,05 m/s.

Therefore, the convergence criteria were updated so as to have enough iterations for the cells in the upper tank region of the control domain to transmit information, namely temperature, down to the very end of the control volume, as well as to achieve convergence as intended. The new convergence criteria are presented in Table 5.4. With this new criteria, similar simulations were performed again with the same HTF initial velocity conditions.

Table 5.4: Updated values of the residuals for the convergence criteria.

Continuity	x	y	Energy	k	ω
10e-4	10e-4	10e-4	10e-6	10e-4	10e-4

Figures 5.6 and 5.7 show the temperature curve along the symmetry and 0.7 m from the symmetry respectively.

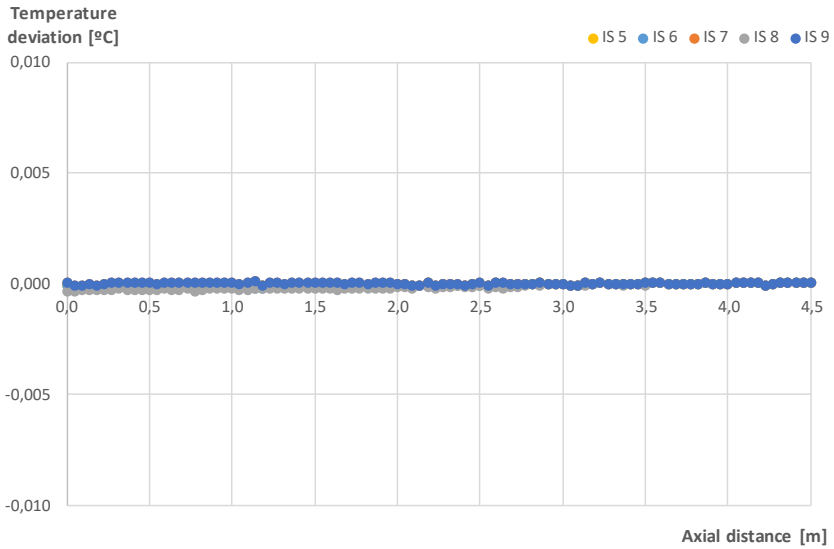

Figure. 5.6: Temperature profile along the symmetry of the tank with different initial solutions (IS) with regard to y-velocity.

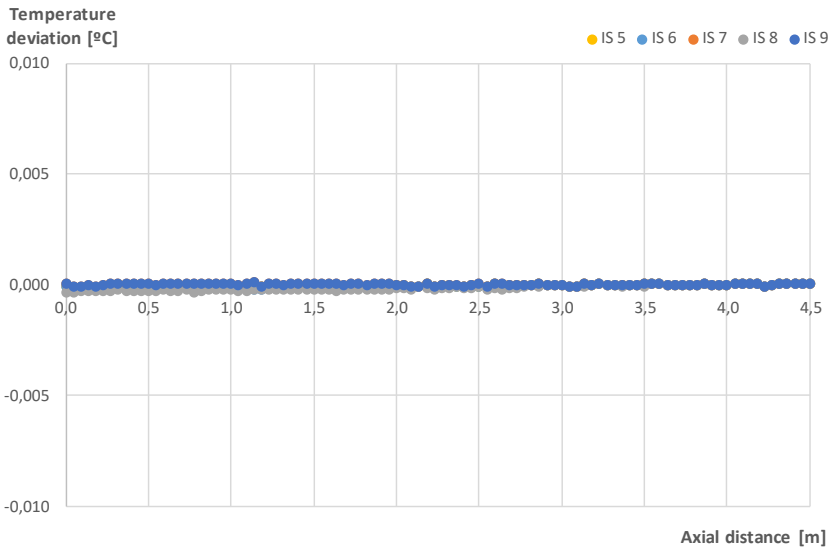

Figure. 5.7: Temperature profile along a distance of 0,7 m from the symmetry axis with different initial solutions (IS) with regard to y-velocity.

Figures 5.6 and 5.7 show the temperature profiles very close to 500 °C with fluctuation in the range of 10e-4. Hence,it can be concluded that the initial velocites did not affect the end result of the simulations resulting in the realisation of the initial velocity convergence.

The new converge criteria introduced additional computational effort. Thus, in Table 5.5 the new computational effort is reported with regard to the reference case considered in Table 4.2.

Table 5.5: Computational effort considering the new convergence criteria.

	y-velocity (m/s)	Relative time
IS 5	-0,005	472,1%
IS 6	-0,05	554,9%
IS 7	-0,5	854,9%
IS 8	-5	1 277,0%
IS 9	5	1 200,8%
IS 10	0,005	490,2%

Finally, when considering the results in terms of velocity profiles in symmetry axis, some increase in velocity can be found in the vicinity of the symmetry axis, this increase in velocity was not expected and eventually it represents the propagation of a numerical artifact passing from one side to other of the symmetry plane (Figure 5.8). Therfore, it was considered to discard the possibility of using the symmetry axis, which was initially considered in order to reduce by half the number of

cells, thus reducing the computational time. Hence, the geometry defined for the final dimensions will be fully defined in order to avoid mathematical distortions.

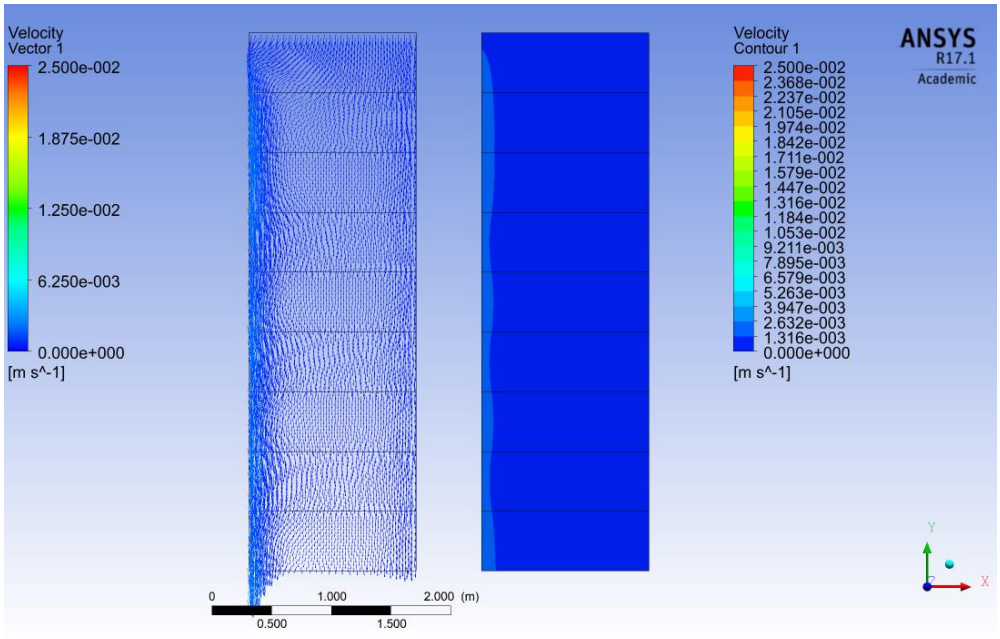

Figure. 5.8: Velocity profile and velocity contours along the symmetry axis considering. IS 5.